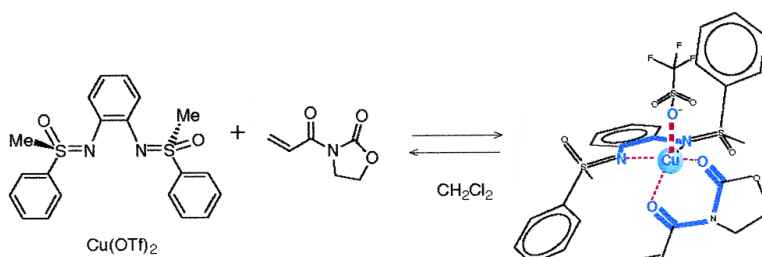Article

Spectroscopic Investigations of Bis(sulfoximine) Copper(II) Complexes and Their Relevance in Asymmetric Catalysis

Carsten Bolm, Marc Martin, Georg Gescheidt, Cornelia Palivan, Dmytro Neshchadin, Helmut Bertagnolli, Martin Feth, Arthur Schweiger, George Mitrikas, and Jeffrey Harmer

More About This Article

Additional resources and features associated with this article are available within the HTML version:

- Supporting Information
- Links to the 5 articles that cite this article, as of the time of this article download
- Access to high resolution figures
- Links to articles and content related to this article
- Copyright permission to reproduce figures and/or text from this article

View the Full Text HTML

Spectroscopic Investigations of Bis(sulfoximine) Copper(II) Complexes and Their Relevance in Asymmetric Catalysis

Carsten Bolm,*,† Marc Martin,† Georg Gescheidt,*,‡ Cornelia Palivan,‡
Dmytro Neshchadin,‡ Helmut Bertagnolli,*,§ Martin Feth,§ Arthur Schweiger,*,‖
George Mitrikas,‖ and Jeffrey Harmer‖

*Contribution from the Institut für Organische Chemie der RWTH Aachen, Prof.-Pirlet-Strasse 1,
D-52056 Aachen, Germany, Institut for Physical Chemistry, University of Basel,
Klingelbergstrasse 80, CH-4056 Basel, Switzerland, Institut für Physikalische Chemie der
Universität Stuttgart, Pfaffenwaldring 55, D-70569 Stuttgart, Germany, and Laboratory of
Physical Chemistry, ETH Hönggerberg, HCI, CH-8093 Zürich, Switzerland*

Received July 26, 2002; E-mail: georg.gescheidt@unibas.ch

Abstract: The structure of Cu(II) complex **3** formed within the course of a stereoselective Diels−Alder reaction was investigated by EXAFS, CW-EPR at X- and W-band, HYSCORE, pulsed ENDOR, and UV−vis spectroscopy. The experimental techniques indicate that the chiral bis(sulfoximine) ligand (*S,S*)-**1** and the dienophile form a tetragonally distorted complex in CH_2Cl_2. The ligand binds to the Cu(II) center via the imine nitrogens, whereas the dienophile interacts via the carbonyl oxygen atoms. The additional sites of the first coordination sphere are occupied by counterions and, presumably, solvent molecules. At the axial position, a triflate anion binds via an oxygen atom.

Introduction

Asymmetric metal catalysis is an attractive field of organic synthesis.[1−6] Products with excellent enantioselectivities have been obtained using catalysts with well-defined chiral ligands. Besides diphosphines, chelating compounds with nitrogens as donor atoms have been given significant attention.[3,7−18] Recently, we introduced bis(sulfoximines) as a new class of C_2-symmetric chelating agents and reported that copper(II) complexes with (*S,S*)-**1** as the ligand were capable of catalyzing asymmetric hetero-Diels−Alder (HDA) reactions,[19,20] affording products with enantioselectivities up to 99% ee.[21,22] Related bis(sulfoximines) were found to serve as effective ligands in copper-catalyzed Diels−Alder (DA) reactions[23] and palladium-catalyzed allylic alkylations.[24,25]

What is the pathway of such stereoselective C−C bond-forming reactions? How do the reactants bind to the catalytically active complex, and do the solvent and the negatively charged counterions participate? Obviously, such questions cannot be answered by crystal-structure analysis because crystals of molecular assemblies consisting of a metal complex, counterions, solvent molecules, and, importantly, substrates can hardly be obtained. Moreover, it is questionable if a solid-state arrangement of molecules mirrors the experimental conditions present in a solution.

Here we present some insight into the changes in the ligand sphere within the course of the catalytic DA reaction catalyzed by the Cu(II) complex of (*S,S*)-**1**.

To obtain insight into the stepwise changes of the ligand sphere, we will first describe the solvent-free complex [Cu(II)-(*S,S*)-**1**(OTf)$_2$] on the basis of EXAFS measurements. The alteration of the ligand sphere around the paramagnetic Cu(II)

† RWTH Aachen.
‡ University of Basel.
§ Universität Stuttgart.
‖ ETH Zürich.
(1) Noyori, R. *Asymmetric Catalysis in Organic Synthesis*; Wiley: New York, 1994.
(2) Ojima, I., Ed. *Catalytic Asymmetric Synthesis*, 2nd ed.; VCH Publisher: New York, 2000.
(3) Jacobsen, E. N., Pfaltz, A., Yamamoto, H., Eds. *Comprehensive Asymmetric Catalysis*; Springer: Berlin, 1999.
(4) Beller, M., Bolm, C., Eds. *Transition Metals for Organic Synthesis*; Wiley-VCH: Weinheim, 1998.
(5) Brunner, H.; Zettlmeier, W. *Handbook of Enantioselective Catalysis*; VCH: Weinheim, 1993; Vols. I and II.
(6) Bolm, C.; Muñiz, K. *Chem. Soc. Rev.* **1999**, *28*, 51−59.
(7) Togni, A.; Venanzi, L. M. *Angew. Chem.* **1994**, *106*, 517−547.
(8) Fache, F.; Schulz, E.; Tommasino, M. L.; Lemaire, M. *Chem. Rev.* **2000**, *100*, 2159−2231.
(9) Pfaltz, A. *Chimia* **1990**, *44*, 202−213.
(10) Pfaltz, A. *Acc. Chem. Res.* **1993**, *26*, 339−345.
(11) Pfaltz, A. *Acta Chem. Scand.* **1996**, *50*, 189−194.
(12) Pfaltz, A. *Synlett* **1999**, 835−842.
(13) Ghosh, A. K.; Mathivanan, P.; Cappiello, J. *Tetrahedron: Asymmetry* **1998**, *9*, 1−45.
(14) Evans, D. A.; Rovis, T.; Johnson, J. S. *Pure Appl. Chem.* **1999**, *71*, 1407−1415.
(15) Johnson, J. S.; Evans, D. A. *Acc. Chem. Res.* **2000**, *33*, 325−335.
(16) Jacobsen, E. N.; Wu, M. H. In *Comprehensive Asymmetric Catalysis*; Jacobsen, E. N., Pfaltz, A., Yamamoto, H., Eds.; Springer: Berlin, 1999; p 649.
(17) Katsuki, T. In *Catalytic Asymmetric Synthesis*, 2nd ed.; Ojima, I., Ed.; VCH: New York, 2000; p 287.
(18) Dalton, C. T.; Ryan, K. M.; Wall, V. M.; Bousquet, C.; Gilheany, D. G. *Top. Catal.* **1998**, *5*, 75.

(19) Jørgensen, K. A. *Angew. Chem., Int. Ed.* **2000**, *39*, 3558−3588.
(20) Jørgensen, K. A.; Johannsen, M.; Yao, S.; Audrain, H.; Thorhauge, J. *Acc. Chem. Res.* **1999**, *32*, 605−613.
(21) Bolm, C.; Simic, O. *J. Am. Chem. Soc.* **2001**, *123*, 3830−3831.
(22) Bolm, C.; Bienewald, F.; Harms, H. *Synlett* **1996**, 775−776.
(23) Bolm, C.; Martin, M.; Simic, O.; Verrucci, M. *Org. Lett.* **2003**, *5*, 427−429.
(24) Bolm, C.; Simic, O.; Martin, M. *Synlett* **2001**, 1878−1880.
(25) Harmata, M.; Ghosh, S. K. *Org. Lett.* **2001**, *3*, 3321−3323.

Table 1. Structural Parameters of Solid $Cu(OTf)_2$ and the Isolated Solid Products of $Cu(OTf)_2 + (S,S)$-**1** in THF Determined from the Cu K-edge EXAFS Spectrum[a]

		r [Å]	N	σ [Å]	ΔE_0 [eV]	k-range [Å^{-1}] fit-index
$Cu(OTf)_2$	Cu−O	1.95 ± 0.02	4.0 ± 0.4	0.063 ± 0.006	17.1	3.20−12.90 14.0
$Cu(OTf)_2$ + 1 equiv of (S,S)-**1**	Cu−N/O	1.97 ± 0.02	4.4 ± 0.4	0.076 ± 0.006	24.5	3.20−12.90 22.5
$Cu(OTf)_2$[26]	Cu−O	1.96	4	0.084		

[a] Absorber-backscatterer distance r, coordination number N, Debye−Waller factor σ with their calculated deviation, shift of the energy threshold ΔE_0, and the fit-index R (AFAC = 0.8).
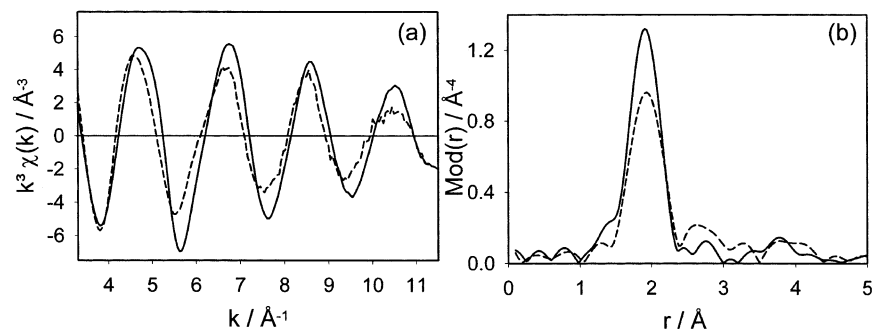
Figure 1. Comparison of the experimental $k^3 \chi(k)$-functions (a) and their Fourier transforms (b) of solid $Cu(OTf)_2$ (solid line), the isolated solid product of $Cu(OTf)_2$ + 1 equiv of the (S,S)-**1** in THF (dashed line).

Scheme 1
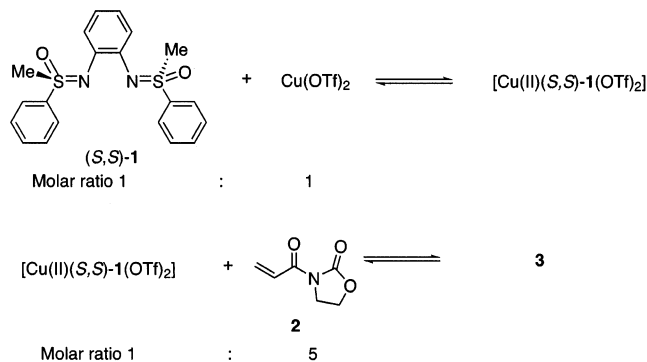
center upon addition of the solvent (CH_2Cl_2) and upon the introduction of dienophile **2** forming complex **3** (Scheme 1) will then be followed by electron paramagnetic resonance (EPR) techniques and UV−vis spectroscopy. This procedure is accomplished under the same experimental conditions as the catalytic reaction is carried out. This ensures that the physicochemical measurements are performed under "authentic" conditions.

Results

EXAFS Spectroscopy of [Cu(II)(S,S)-1(OTf)$_2$]. The structure determination by EXAFS spectroscopy is an ideal basis to obtain information about the reaction depicted in Scheme 1. Because the solvent is completely removed during the preparation of the sample, the geometry of the pure amorphous complex [Cu(II)(S,S)-**1**(OTf)$_2$] is obtained and the consecutive modifications of the ligand sphere by the solvent and substrate **2** are followed step by step.

The structural parameters determined by Cu K-edge EXAFS spectroscopy of solid $Cu(OTf)_2$ and the resulting product with (S,S)-**1** are summarized in Table 1. Figure 1a shows the experimental k^3-weighted $\chi(k)$-functions, and Figure 1b shows

the corresponding Fourier transforms (FT) in r-space of both compounds. The FT $k^3 \chi(k)$-function of $Cu(OTf)_2$ exhibits one main peak in the range of 1.9−2.0 Å. Therefore, the EXAFS function was fitted with a one-shell model. This shell can be assigned to the coordinating oxygen atom of the triflate anions. The Cu−O distance amounts to 1.95 Å with a determined coordination number of 4.0. This result reveals a tetracoordinated Cu(II) in $Cu(OTf)_2$ pointing to four formally equivalent oxygen atoms in a square planar arrangement in agreement with published data.[26]

Introduction of ligand (S,S)-**1** leads to a significantly distinguishable decrease of the experimental $k^3 \chi(k)$-function in comparison with that of the parent $Cu(OTf)_2$. Also, in the Fourier transform, the main peak is much lower, indicating the changes between the two compounds. This fact can be explained by the replacement of two oxygen atoms by two nitrogens, which have nearly the same but somewhat lower backscattering amplitude than oxygen atoms. Accordingly, the Cu(II) ion in [Cu(II)(S,S)-**1**(OTf)$_2$] is surrounded by the two imine nitrogens and two triflate oxygens. The mean distance of all surrounding atoms was determined as 1.97 Å; this value is compatible with a distorted square planar coordination geometry of the copper central atom. A further indication for a square planar or slightly distorted geometry of the Cu(II) cations in $Cu(OTf)_2$ and [Cu(II)(S,S)-**1**(OTf)$_2$] is the absence of the 1s → 3d pre-peak in the XANES region of the X-ray absorption spectra for both compounds. As tetrahedral Cu(II) complexes should show a small, but clearly detectable, 1s → 3d pre-peak,[27] a tetrahedral coordination geometry of Cu(II) in $Cu(OTf)_2$ and [Cu(II)(S,S)-**1**(OTf)$_2$] is unlikely.

UV−Vis Spectra and EPR Techniques. The formation of complex [Cu(II)(S,S)-**1**(OTf)$_2$] in solution can be followed by a shift of the metal centered d−d band in the UV−vis spectrum

(26) Boumizane, K.; Herzog-Cance, M. H.; Jones, D. J.; Pascal, J. L.; Potier, J.; Roziere, J. *Polyhedron* **1991**, *10*, 2757−2769.
(27) Sano, M.; Komorita, S.; Yamatera, H. *Inorg. Chem.* **1992**, *31*, 459−463.
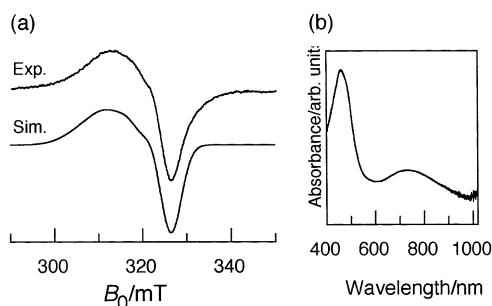
Figure 2. (a) Fluid-solution X-band EPR spectrum of complex **3** (*T* = 298 K) and the corresponding simulation. (b) UV−Vis spectrum recorded simultaneously with the EPR spectrum.
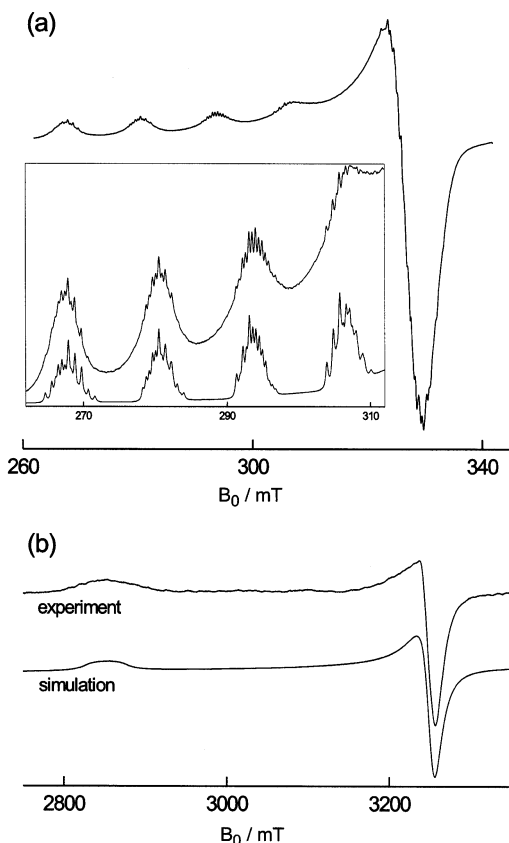
Figure 3. Frozen-solution EPR spectra of complex **3** and the corresponding simulations. (a) X-band (*T* = 120 K). Inset: $g_{\parallel}$ region showing the copper and ligand hyperfine splittings. Upper trace, experiment; lower trace, simulation. (b) W-band FID-detected EPR spectrum (*T* = 20 K, first derivative).

from 640 to 710 nm when (*S,S*)-**1** is added to parent Cu(OTf)$_2$ in CH$_2$Cl$_2$ (1:1 molar ratio). In parallel, the patterns of the EPR spectra in fluid and in frozen solution (room temperature and 77 K) undergo substantial transformations, indicating that the ligand has coordinated with the Cu(II) ion. Broad features in the EPR spectra of [Cu(II)(*S,S*)-**1**(OTf)$_2$] reveal a poorly defined coordination sphere. Upon addition of dienophile **2**, the d−d band is further shifted from 710 to 725 nm (Figure 2).

The frozen-solution EPR signals at X- and W-band (Figure 3) bear out the formation of complex **3** (Scheme 1) with a well-defined geometry. A remarkably well-resolved ligand hyperfine structure, particularly along $g_{\parallel}$, is observed in the frozen-solution spectrum (Figure 3a). However, because CH$_2$Cl$_2$ has the tendency to form microcrystallites upon freezing, the powder

Table 2. *g* and ^{63}Cu Hyperfine Principal Values (*A*/MHz) and UV−Vis Absorption Bands (abs/nm) Attributed to Complex **3**

	$g_{\perp}$	$g_{\parallel}$	g_{iso}	$|A_{\perp}|$	$|A_{\parallel}|$	$|A_{iso}|$	abs
frozen soln.	2.068	2.357		23	410		
fluid soln.			2.169			121.4	449
							592 (sh)
							726

spectrum is slightly deteriorated by the contributions of the dominating microcrystals. These unwanted features have been eliminated by summing up spectra recorded with different orientations of the sample with respect to the magnetic field.

The W-band EPR spectrum shown in Figure 3b indicates that the **g** matrix is axial even with the high resolution obtained at 94.1 GHz. A successful simulation (Figure 3a) of the experimental ligand hyperfine structure along $g_{\parallel}$ is accomplished, taking into account two nitrogen nuclei with hyperfine values, $A_{\parallel}$, of ca. 30 MHz. The *g* and copper hyperfine principal values determined from the X- and W-band spectra and utilized for the spectral simulations are listed in Table 2. When the EPR parameters determined from the frozen-solution spectra were used to calculate the corresponding isotropic values, the fluid-solution EPR signal was simulated in a straightforward way (see Figure 2). Moreover, several freeze−thaw procedures of the samples always yielded identical frozen- and fluid-solution EPR spectra. Therefore, we conclude that complex **3** possesses identical geometry in both the liquid and the frozen solution.

Further insight into the nature of the ligand atoms is provided by using pulsed EPR and ENDOR spectroscopy[28,29] at X- and W-band. Hyperfine-contrast selective Davies-ENDOR spectra at X-band (Figure 4a) show both proton and nitrogen signals. With weak and long microwave pulses, the proton signals dominate (traces 1 and 3), whereas with strong and short microwave pulses, the signals of the weakly coupled ^{1}H nuclei are attenuated, and the nitrogen signals centered at approximately *A*/2 become dominant (traces 2 and 4). These data reveal ^{14}N hyperfine couplings between 29 and 34 MHz (depending upon the orientation), values which are in agreement with the ligand hyperfine splittings observed in the frozen solution X-band EPR spectrum (Figure 3a) and which are typical of equatorially coordinated nitrogen nuclei with the unpaired electron in the d$_{x^2−y^2}$ orbital of the Cu(II) ion.

The hyperfine interactions of the ^{19}F nuclei of a triflate ligand are observed with Mims-ENDOR at W-band (Figure 4b). In this figure, both traces have been centered around the ^{19}F Larmor frequency, ν_{19_F}. The orientation-dependent ^{19}F hyperfine interaction (1.3 MHz along $g_{\parallel}$ and 0.57 MHz along $g_{\perp}$) is used to estimate the distance and orientation between the Cu(II) cation and the fluorine nuclei. Assuming a negligible isotropic contribution to the hyperfine interaction and using the point-dipole approximation with the dipole coupling constant

$$T = \frac{\mu_0}{4\pi}\frac{g\beta_e g_n\beta_n}{h}\frac{1}{r^3}$$

where *r* is the distance, we find a value of *T* = 0.57 MHz,

(28) Gemperle, C.; Schweiger, A. *Chem. Rev.* **1991**, *91*, 1481−1505.
(29) Schweiger, A.; Jeschke, G. *Principles of Pulse Electron Paramagnetic Resonance*; Oxford University Press: Oxford, 2001.

a)

b)
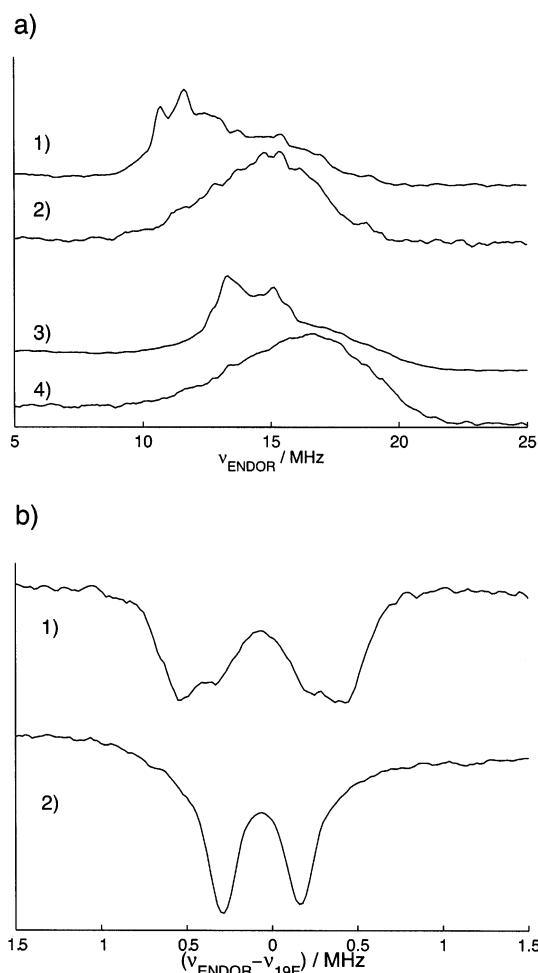
Figure 4. (a) Hyperfine contrast selective X-band Davies-ENDOR spectra measured near $g_\parallel$ (traces 1 and 2) and $g_\perp$ (traces 3 and 4). Traces 1 and 3 use a π pulse of length 200 ns; traces 2 and 4 use a π pulse of length 32 ns to suppress the weakly coupled protons. The strongly coupled ^{14}N nuclei (trace 2 and 4) are centered at one-half of the hyperfine coupling, $A/2$, between 14.5 and 17 MHz. (b) ^{19}F W-band Mims-ENDOR spectra measured at $g_\parallel$ (trace 1) and $g_\perp$ (trace 2). For further details, see Experimental Section.

which corresponds to $r \approx 500$ pm with the fluorines located near the $g_\parallel$ axis (axial position). Thus, at least one of the triflate anions is located in an axial position close to the Cu(II) ion.

In the HYSCORE experiment of **3**,[29] taken along $g_\parallel$, several interactions between the Cu(II) cation and adjacent magnetic nuclei become discernible (Figure 5). Along the main diagonal representing the nuclear Larmor frequencies, several couplings with ^{1}H, ^{19}F, ^{13}C, ^{14}N, and, very likely, of ^{35}Cl/^{37}Cl nuclei are apparent. Close to the antidiagonal at 11.70 MHz, resonances of strongly coupled protons ($A(^1$H$) \leq 10$ MHz) appear. They are tentatively assigned to the protons in the sulfoximine ligand (S,S)-**1**. Because these couplings are not resolved in the EPR signals and their multiplicities are, therefore, not discernible, they cannot be assigned to specific positions. In addition, at lower frequencies (<5 MHz), peaks which can be assigned to ^{13}C nuclei in natural abundance ($A(^{13}$C$) \leq 5$ MHz), the remote ^{14}N nucleus of ligand **2**, and/or chlorine atoms of the CH$_2$Cl$_2$ solvent are observed. The ^{19}F coupling of 1.3 MHz along $g_\parallel$ already detected by Mims-ENDOR also emerges in the HY-SCORE spectrum.
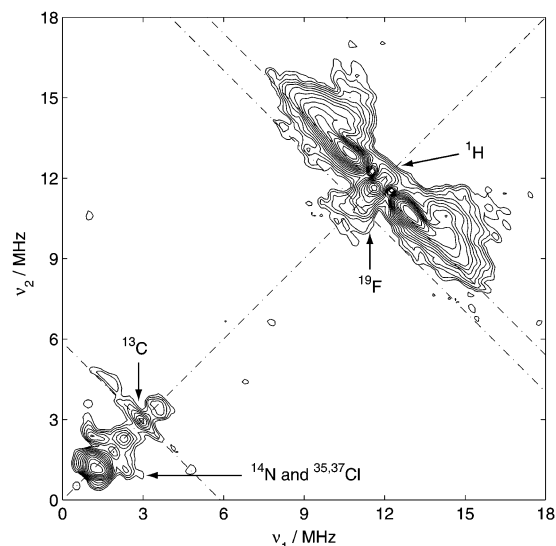
Figure 5. HYSCORE spectrum of **3**. Measured along $g_\parallel$; $T = 20$ K. The positions of the Larmor frequencies of the ^{1}H, ^{19}F, and ^{13}C, and the region of ^{14}N, ^{35}Cl, and ^{37}Cl, are indicated in the graph. For further details, see the Experimental Section.

Structural Considerations

Starting from a nearly square planar geometry of solvent-free [Cu(II)(S,S)-**1**(OTf)$_2$], the catalytically active complex undergoes considerable reorganizations in the course of the catalytic procedure. Addition of the solvent (CH$_2$Cl$_2$) leads to a highly fluxional species. Addition of substrate **2** leads to the well-defined complex **3** (Scheme 1), and from the EPR data and UV−vis spectra, a structural model for this complex can be derived. The g values given in Table 2 are in line with the unpaired electron being in a d$_{x^2-y^2}$ orbital. They point to either a square pyramidal, a square planar, or an elongated tetragonal symmetry.[30] A more precise distinction between these geometries can be drawn by comparison with parameters from related Cu(II) complexes. A recent example is the complex of N,N'-bis(glycine-2-benzimidazolyl)hexanediamide, a tetradentate ligand which binds to Cu(II) via two amide nitrogen and two carbonyl oxygen atoms, forming the main plane of a tetragonal pyramid with a chloride ion occupying the axial site.[31] The structure of this complex has been established by X-ray analysis of the corresponding single crystals, UV−vis, and EPR spectroscopy. The $g_\perp$ and $g_\parallel$ values of 2.07 and 2.33, respectively, are almost identical to those of **3** (Table 2), verifying the d$_{x^2-y^2}$ orbital. Moreover, the $|A_\parallel|$ value of 406 MHz matches that of **3**. These EPR parameters together with the broad d−d band at around 740 nm (**3**: 725 nm) are distinctive for a tetragonal site being present in fluid solution. Tetragonally distorted complexes still have axial **g** and copper hyperfine matrixes, but in comparison to square planar Cu(II) complexes they typically have higher $g_\parallel$ and lower $A_\parallel$ values.[32] An example is [Cu(bis(2-benzimida-zolyl)-propane)$_2$](ClO$_4$)$_2$(1-PropOH)(H$_2$O) with $g_\parallel = 2.31$, $g_\perp = 2.07$, and $A_\parallel = 398$ MHz.[33] The data of complex **3** are very

(30) Hathaway, B. J. *Struct. Bonding (Berlin)* **1984**, *57*, 55−118.
(31) Gupta, M.; Mathur, P.; Butcher, R. J. *Inorg. Chem.* **2001**, *40*, 878−885.
(32) Sakaguchi, U.; Addison, A. W. *J. Chem. Soc., Dalton Trans.* **1979**, 600−608.
(33) van Albada, G. A.; Smeets, W. J. J.; Veldman, N.; Spek, A. L.; Reedijk, J. *Inorg. Chim. Acta* **1999**, *290*, 105−112.
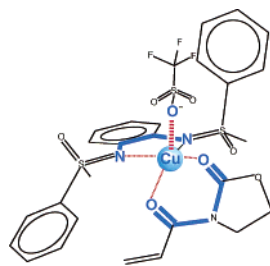
Figure 6. Sketch for the geometry of complex **3** in CH_2Cl_2 based on EPR and UV−vis spectroscopy. Directly interacting ligand atoms are presented in blue.

similar, and these values are therefore again consistent with a tetragonally distorted structure. This geometry is corroborated by the broad band at 726 nm in the UV−vis spectrum.

Thus, two N and two O atoms form the main (distorted) plane of Cu(II) complex **3**. The ^{14}N hyperfine coupling constants (in the order of 30 MHz, see above), determined by Davies-ENDOR and EPR simulations, confirm this assignment.[34] The fifth coordination site is occupied by a triflate anion interacting via oxygen. This is borne out by the ^{19}F resonances in the W-band ENDOR because the calculated value of 500 pm agrees with the average distance between the copper and the fluorines of a triflate anion, assuming that the triflate coordinates axially to Cu(II) via O^- (according to a provisional molecular-mechanics calculation; see Figure 6). The association with triflate anions in the course of Cu(II)-catalyzed reactions has been discussed in the case of aldol reactions,[35] and it was frequently observed that the nature of the counterions plays an important role for the stereoselectivity.[36,37] The detection of the low-frequency signals in the HYSCORE experiments (Figure 5) points to the solvent participating as an additional weakly bound ligand (presumably via the Cl atoms). The geometry of **3** anticipated from the above experimental results is sketched in Figure 6.

Conclusions

In summary, the above spectroscopic results clearly demonstrate that a distorted, nonsymmetric square pyramidal geometry exists for **3**, which is the primarily formed complex between the catalyst [Cu(II)(*S*,*S*)-**1**(OTf)$_2$] and substrate **2**. It has been experimentally established that in the first stage of the catalytic pathway at least one triflate anion is directly participating in the first coordination sphere around Cu(II) by occupying an axial site.

Selective deuteration of the ligand methyl and phenyl groups of (*S*,*S*)-**1** will enable us to determine the orientation of these substituents in the complex. Furthermore, we intend to obtain additional insight into further stages of Cu(II)-based Lewis-acid-catalyzed reactions utilizing several different ligands. This and model calculations should help to establish the subtle influence of counterions and solvents on the efficiency and stereoselectivity of catalytically induced C−C bond-forming reactions.

Experimental Section

EXAFS. Parent Cu(II) triflate and ligand (*S*,*S*)-**1** were dissolved in CH_2Cl_2 (molar ratio 1:1). After a homogeneous mixture of the components was achieved, the solvent was evaporated in vacuo.

The EXAFS measurements were performed at beamline E4 at the Hamburger Synchrotronstrahlungslabor des Deutschen Elektronensynchrotrons (HASYLAB at DESY, Hamburg, Germany) and at beamline KMC-2 at the Berliner Elektronenspeicherring-Gesellschaft für Synchrotronstrahlung m.b.H (BESSY II, Berlin, Germany). For the measurements at the Cu K-edge (8979.0 eV), a Si(111) double crystal monochromator was used at HASYLAB. At BESSY, a Si(220) double graded-crystal (0.5% Ge/cm) monochromator was used for the copper edge. The tilt of the second monochromator crystal was set to 40% harmonic rejection. Energy resolution was estimated to be about 0.7−1.0 eV at the Cu−K edge. Energy calibration was performed with the corresponding metal foil. The synchrotron beam current was between 80 and 100 mA at HASYLAB (positron energy 4.45 GeV) and between 100 and 250 mA at BESSY (electron energy 1.7 GeV).

All of the experiments were carried out under ambient conditions in transmission mode with ion chambers at 25 °C. All ion chambers were filled with nitrogen in the case of the measurements at the Cu K-edge. The solid samples were embedded in a polyethylene matrix and pressed to pellets. The concentration of all samples was adjusted to yield an absorption jump of $\Delta\mu d \approx 1.5$.

Data evaluation started with background absorption removal from the experimental absorption spectrum by subtraction of a Victoreen-type polynomial. The background-subtracted spectrum was then convoluted with a series of increasingly broader Gauss functions, and the common intersection point of the convoluted spectra was taken as energy E_0.[38,39] To determine the smooth part of the spectrum, corrected for preedge absorption, a piecewise polynomial was used. It was adjusted in such a way that the low-*R* components of the resulting Fourier transform were minimal. After division of the background-subtracted spectrum by its smooth part, the photon energy was converted to photoelectron wavenumbers *k*. The resulting EXAFS function was weighted with k^3. Data analysis in *k* space was performed according to the curved wave multiple scattering formalism of the program EX-CURV92 with XALPHA phase and amplitude functions.[40] The mean free path of the scattered electrons was calculated from the imaginary part of the potential (VPI was set to −4.00), and an overall energy shift (ΔE_0) was assumed. The amplitude reduction factor (AFAC) was set to a value of 0.8.

EPR (X- and W-band Measurements). In dry CH_2Cl_2, 9.4 mg of Cu(OTf)$_2$ was suspended under nitrogen. The ligand (*S*,*S*)-**1** was then added (10 mg, 1:1 molar ratio vs the Cu(II) salt). The solution was kept under nitrogen and stirred for ca. 30 min until the complex [Cu-(II)(*S*,*S*)-**1**(OTf)$_2$] was formed. **2** was then added in 5-fold molar excess to [Cu(II)(*S*,*S*)-**1**(OTf)$_2$] under nitrogen. This solution was transferred into the EPR sample tube under inert gas. The sample was then degassed by three freeze−pump−thaw cycles under high vacuum and sealed. Five samples were prepared by this procedure and gave identical EPR spectra. The presence of moisture immediately leads to the decay of the signals for complex **3**.

Continuous wave (CW) EPR measurements were performed on a Bruker ESP300 X-band spectrometer equipped with a rectangular TE$_{102}$ cavity and on a Bruker E500 spectrometer equipped with a super-high Q cavity. EPR spectral simulations were carried out with the program SimFonia (Bruker). During the EPR measurements in fluid solution in situ, UV−vis spectra were taken on a diode-array fiber-optics spectrometer (J&M, Aalen, Germany).[41]

(34) Iwaizumi, M.; Kudo, T.; Kita, S. *Inorg. Chem.* **1986**, *25*, 1546−1550.
(35) Evans, D. A.; Kozlowski, M. C.; Murry, J. A.; Burgey, C. S.; Campos, K. R.; Connell, B. T.; Staples, R. J. *J. Am. Chem. Soc.* **1999**, *121*, 669−685.
(36) Thorhauge, J.; Roberson, M.; Hazell, R. G.; Jørgensen, K. A. *Chem.-Eur. J.* **2002**, *8*, 1888−1898.
(37) Evans, D. A.; Johnson, J. S.; Olhava, E. J. *J. Am. Chem. Soc.* **2000**, *122*, 1635−1649.

(38) Ertel, T. S.; Bertagnolli, H.; Hückmann, S.; Kolb, U.; Peter, D. *Appl. Spectrosc.* **1992**, *46*, 690−698.
(39) Newville, M.; Livins, P.; Yakoby, Y.; Rehr, J. J.; Stern, E. A. *Phys. Rev. B* **1993**, *47*, 14126−14131.
(40) Gurman, S. J.; Binsted, N.; Ross, I. *J. Phys. C* **1986**, *19*, 1845−1861.
(41) Gescheidt, G. *Rev. Sci. Instrum.* **1994**, *65*, 2145−2146.

Pulse EPR experiments at X-band were carried out on a Bruker E580 spectrometer (mw frequency 9.68 GHz) at 20 K. Measurements at W-band (94.1 GHz) were carried out on a Bruker E680 spectrometer (mw frequency 94.1 GHz) between 8 and 20 K. Davies-ENDOR experiments at X-band were carried out with the pulse sequence $\pi - T - \pi/2 - \tau - \pi - \tau - $ echo. One sequence employed a π ($\pi/2$) pulse of length 200 (100) ns, and the second sequence employed a π ($\pi/2$) pulse of length 32 (16) ns (hyperfine contrast selectivity to suppress the spectral features of weakly coupled protons). A radio frequency pulse with a length of 10 μs was used. Mims-ENDOR experiments were carried out at W-band using the pulse sequence $\pi/2 - \tau - \pi/2 - T - \pi/2 - \tau - $ echo, with a $\pi/2$ pulse of length 200 ns and a radio frequency pulse of length 15 μs. The field-swept EPR spectrum was recorded via the FID following a pulse length of 800 ns.

The HYSCORE experiment was carried out using the pulse sequence $\pi/2 - \tau - \pi/2 - t_1 - \pi - t_2 - \pi/2 - \tau - $ echo with mw pulses of length $t_{\pi/2} = t_{\pi} = 16$ ns, a τ value of 158 ns, a starting time of 96 ns for t_1 and t_2, and a time increment $\Delta t = 12$ ns (data matrix 350 × 350); an eight-step phase cycle was used. The experiment was done at 20 K at the observer position of 274.9 mT with a microwave frequency of 9.68 GHz.

JA027870W